J Mol Model (2013) 19:3569–3580
DOI 10.1007/s00894-013-1872-2

ORIGINAL PAPER

Modeling the physisorption of bisphenol A on graphene and graphene oxide

Diego Cortés-Arriagada · Luis Sanhueza · Mireya Santander-Nelli

Received: 12 December 2012 / Accepted: 30 April 2013 / Published online: 31 May 2013

Abstract The physisorption of bisphenol A (BPA) on pristine and oxidized graphene was studied theoretically via calculations performed at the PBE-D3 level (including dispersion force corrections). Three stable conformations of BPA on graphene were found. A lying-down configuration was energetically favored because the presence of π–π stacking and dispersion forces increased interactions. In addition, the adsorption of BPA on the edges of graphene oxide was enhanced when adsorption occurred on carboxyl and carbonyl groups, whereas the adsorption strength decreased when adsorption occurred on hydroxyl groups. The highest physisorption strength was obtained on the surface of graphene oxide due to the presence of π–π stacking and dispersion forces (which provided the greatest contribution to the adsorption energy) as well as hydrogen bonds (which provided a smaller contribution), indicating that oxidized graphene is a better candidate than pristine graphene for BPA removal. On the other hand, an increase in electrophilicity was observed after the physisorption of BPA in all systems (with respect to graphene and BPA in their isolated forms), with the adsorbent acting as the electron acceptor. Finally, molecular dynamics simulations performed using the PM6 Hamiltonian showed that the adsorption of BPA on graphene is stable.

Keywords Graphene · Graphene oxide · Bisphenol A · DFT-D3

Introduction

Bisphenol A (BPA), 2,2-bis(4-hydroxyphenyl)propane, is a common chemical utilized in the production of polycarbonates and epoxy resins, and to line tin cans and harden plastic. Because of its widespead use, BPA is present in a wide variety of products used as food containers (bottled foods and beverages, baby and water bottles, and beverage and food cans). In addition, industrial activity (such as that associated with the paper industry) results in the discharge of BPA as a waste product into the water system, meaning that BPA is found in (ground and surface) water effluents and drinking water [1–3]. At the same time, BPA is an important pollutant that can impact animal and human health because it is an endocrine-disruptor chemical (EDC). BPA has been linked to prostate and breast cancer, birth defects, miscarriages, obesity, premature development in girls, polycystic ovarian syndrome, and hypertension, among other conditions [4–10]. The hazard represented by BPA pollution became more widely known in 2011 when the European Commission banned the manufacture of baby bottles containing BPA in the European Union [11]. The elaboration of processes allowing the control/detection of BPA in the environment is therefore an important task: some recently developed techniques for removing and/or degrading BPA involve solid-phase extraction [12], adsorption on lignin [13], treatment with bacteria [14], and catalytic or photocatalytic degradation [15, 16].

Recently, graphene (G) and graphene-based systems have been successfully employed for the electrochemical sensing of BPA. Graphene has proven to be an incredibly important material, as it possesses unique and useful properties such as high mechanical strength, high thermal and electronic conductivity, and high surface area for the adsorption of

Electronic supplementary material The online version of this article (doi:10.1007/s00894-013-1872-2) contains supplementary material, which is available to authorized users.

D. Cortés-Arriagada (✉) · M. Santander-Nelli
Facultad de Química y Biología, Universidad de Santiago de Chile, Avenida Libertador Bernardo O'Higgins 3363, Estación Central, Santiago, Chile
e-mail: diego.cortesa@usach.cl

L. Sanhueza
Facultad de Química, Pontificia Universidad Católica de Chile, Casilla 306, Santiago, Chile

adsorbates [17–20]. In addition, the conductivity and catalytic activity of graphene is useful in schemes for sensing several organic compounds [21]. Fan et al. prepared an electrochemical sensor of BPA based on nitrogen-doped graphene and chitosan that allowed improved sensing of BPA in river water samples [22]. Ntsendwana and co-workers showed that modifying a glassy carbon electrode with reduced graphene oxide (RGO) improves its electrochemical properties with respect to those of an unmodified electrode; such a sensor was successfully applied to the sensing of BPA in plastic bottles of water [23]. Also, Huang et al. enhanced the electron-transfer kinetics of a glassy carbon electrode by modifying it with a composite containing 3Au–1Pd alloy nanoparticles and graphene. Upon using the improved sensor for the detection of BPA in baby bottles and food storage containers, they found that concentrations of BPA in them were higher than the Chinese Health standard [24].

On the other hand, Xu and co-workers decontaminated an aqueous solution containing BPA using the adsorbent properties of graphene, and obtained higher values of BPA adsorption than achieved with other materials used for BPA removal, such as modified carbon nanotubes and porous carbon. These results show the great potential of graphene for wastewater treatment [25]. FTIR analysis led to the proposal of an adsorption mechanism for BPA on RGO involving π–π electron coupling between the π-electrons of the benzene rings of BPA and RGO, as well as hydrogen-bond interactions between the hydroxyl groups of BPA and the remaining functional groups of RGO before hydrazine treatment [25]. However, in contrast to this abundant experimental data, only a few computational studies have studied the physisorption of BPA on graphene. Zaib and co-workers computed the interaction energies of systems formed upon the adsorption of BPA on a single-walled carbon nanotube (SWCNT) and pristine graphene [26], and found that adsorption on graphene was more favorable than that on SWCNTs because of the planarity of the graphene molecule, which allows for wide overlap with the orbitals of BPA.

In the work described in this paper, we used density functional theory and molecular dynamics calculations to study the physisorption of BPA on pristine and oxidized graphene that was bifunctionalized at its edges and in the bulk. The methodology used involved correction for dispersion forces in the DFT method to achieve an accurate description of vdW interactions. The aim was to obtain adsorption energies of the interaction modes between BPA and graphene adsorbents in order to characterize the physisorption strength and the roles of various functional groups. In addition, the charge, electrostatic potential, and reactivity indices were determined in order to analyze the electronic structure, and molecular dynamics calculations were carried out to check the stability of the physisorption.

Methodology

For all simulations, a finite zigzag graphene lattice containing 25 hexagonal cells was used as the base ($C_{70}H_{22}$); the size of the lattice was ~12.3 × 12.3 Å, and the dangling bonds at the edges were saturated with hydrogen atoms. The "Electronic supplementary material" (ESM) shows that well-converged adsorption energies were obtained on the surface of the $C_{70}H_{22}$. It is important to note that in the research of Xu and co-workers, an adsorption mechanism of BPA on graphene was proposed that accounted for physisorption on the basal plane (bulk) by invoking π–π interactions, and interactions with hydroxyl groups at the graphene edge by means of hydrogen-bond interactions [25]. Therefore, in accordance with [25], we considered two types of graphene systems: (a) pristine graphene, to analyze the physisorption via π–π interactions, and (b) oxidized graphene (functionalized graphene with oxygen-containing functional groups), to study the adsorption involving hydrogen bonding with functional groups in the bulk or edge. In (b), the oxidized graphene systems were built in accordance with experimental data obtained using techniques such as NMR [27, 28], AFM [29, 30], and STM [31], which indicate that hydroxyl and epoxide groups are mainly attached to the basal plane, while the edges are functionalized with carbonyl and carboxyl groups. Since Xu et al. considered hydroxyl groups bonded to the edge of graphene, this configuration was also considered in order to compare it with those determined in the present work.

Scheme 1 shows BPA and the adsorbent systems based on graphene. Considering that the adsorption of BPA is strongly promoted in the presence of two functional groups, only bifunctionalized graphene systems were built: $G^{L\text{-}R\text{-}R}$, where graphene is functionalized at the edge (L), and the R groups are carboxyl, carbonyl, and/or hydroxyl groups; and $G^{R\text{-}R}$, where graphene is functionalized on the basal plane and the R groups are epoxide and/or hydroxyl. Combinations of functional groups were considered. To select the relative positions of the functional groups in bifunctionalized $G^{L\text{-}R\text{-}R}$ and $G^{R\text{-}R}$ adsorbents, geometry optimizations of several models were performed at the semiempirical PM6 level using the package MOPAC2012 [32]; the most stable adsorbents were subsequently used as input for the geometry optimizations performed at the density functional theory (DFT) level.

At the DFT level, the GGA-PBE functional [33, 34] was used due to its relatively low computational cost and good performance for noncovalent interactions of adsorbates on graphene [35–37]; Ahlrichs double-zeta basis set plus one polar set on all atoms was used for Kohn–Sham orbitals. The DFT-D3 method developed by Grimme and co-workers [38] was used for energy and gradients in order to include the effects of dispersion forces in the PBE functional; the corrected PBE functional is the so-called PBE-D3 functional. In the geometry optimizations, the Broyden–Fletcher–Goldfarb–Shanno algorithm was used as the updating

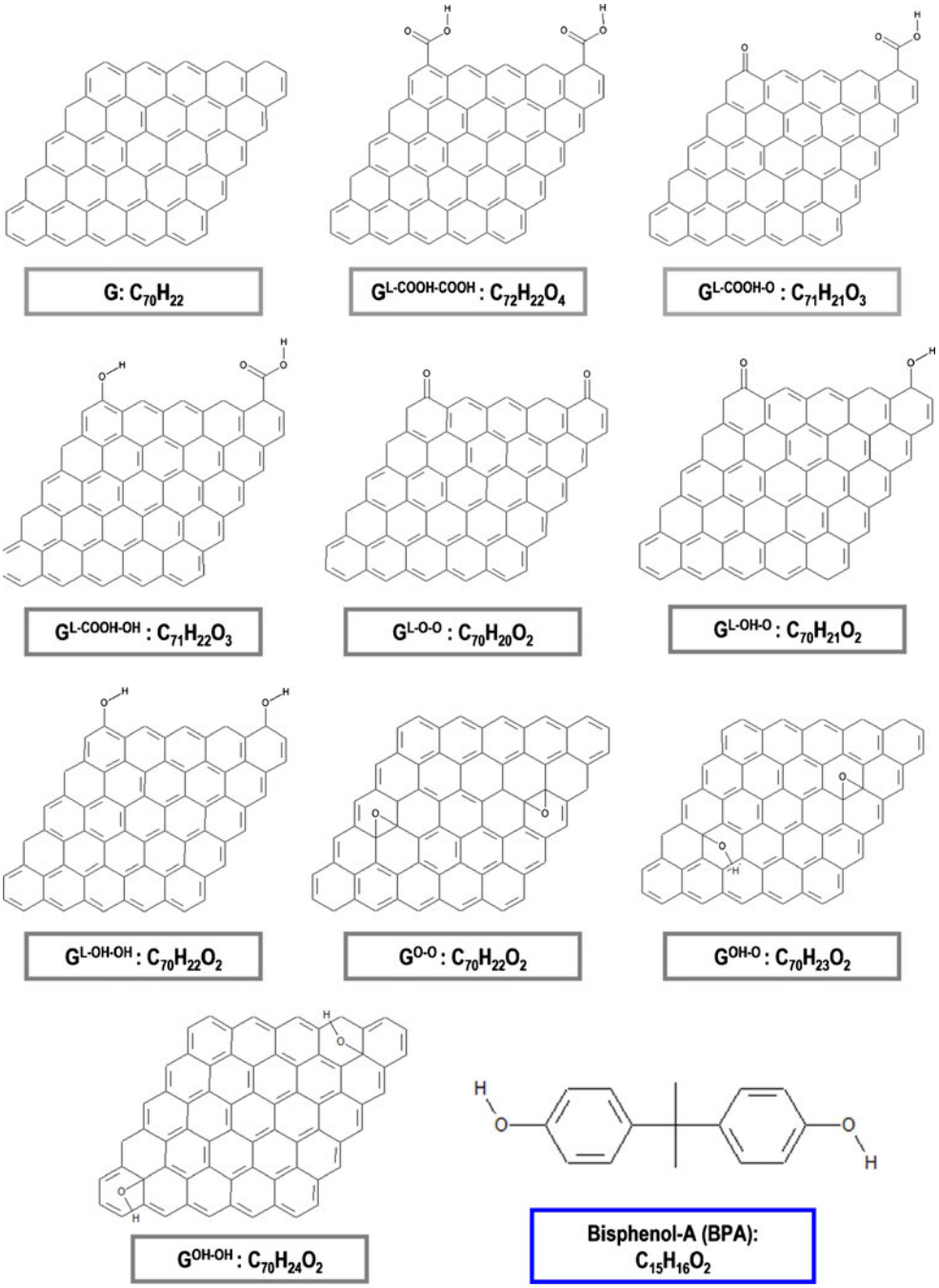

Scheme 1 Structures of bisphenol A (BPA) and the pristine and functionalized (on edges and in the bulk) graphene systems used in the calculations. Hydrogen atoms were removed from the benzene rings (in graphene/BPA) to simplify the calculations

method. Vibrational frequencies were obtained to ensure that the molecular structures optimized at the PBE-D3 level corresponded to energy minima; in all cases, the frequencies were positive. In the geometry optimization and SCF steps, convergence tolerance values of 5×10^{-6} and 1×10^{-8} Eh were used, respectively. DFT calculations were carried out in the electronic structure program ORCA [39]; results were analyzed in the graphical user interface Gabedit [40].

In order to study the performance of the PBE-D3 method, it was applied to study the phenol dimer, and the results were compared with those obtained with the ab initio MP2 method, which explicitly include dispersion effects (see the ESM). Although we wanted to calculate the BPA···graphene system and the BPA dimer, these systems were too computationally expensive to calculate with MP2. However, the methodology used in this work was successfully implemented by us to analyze the adsorption of 4-chlorophenol on graphene [41].

In the analysis, the adsorption energy (AE) was used to characterize the physisorption strength; AE was calculated as:

$$\mathrm{AE} = E_{\mathrm{adsorbent}} + E_{\mathrm{BPA}} - E_{\mathrm{adsorbent-BPA}} - \mathrm{BSSE} \quad (1)$$

where $E_{adsorbent}$, E_{BPA}, and $E_{adsorbent–BPA}$ correspond to the total energies of the adsorbents (pristine or oxidized graphene), BPA, and the adsorbent–BPA system, respectively; BSEE is the energy due to the basis set superposition error, determined via the standard counterpoise correction scheme of Bernardi and Boys [42]. A positive value of AE indicates that the adsorption is exothermic and that the adsorbent–BPA system is stable.

To analyze the charge distribution, charges were obtained from Mulliken population analysis (MPA); also, molecular electrostatic potential (MEP) surfaces were calculated in order to determine sites with negative (red color) or positive (blue color) charge excesses.

On the other hand, the electrophilicity index (ω) was calculated for the isolated and adsorbent–BPA systems in order to characterize changes in electrophilic character. ω corresponds to the energetic stability that reaches a molecular system when it gains electrons, and it is correlated with the electrophilic character of the system [43, 44]. ω was obtained using

$$\omega = \mu^2 \Big/ 2\eta \tag{2}$$

where μ and η are, respectively, the electronic chemical potential and the molecular hardness. These parameters are determined via $\mu \approx (\varepsilon_{LUMO}+\varepsilon_{HOMO})/2$ and $\eta \approx \varepsilon_{LUMO} - \varepsilon_{HOMO}$, respectively, where ε_{LUMO} and ε_{HOMO} correspond to the energies of the lowest unoccupied (LUMO) and the highest occupied (HOMO) molecular orbitals.

Finally, to check the stability of the noncovalent interactions between BPA and graphene (or GO models), molecular dynamics trajectories were carried out via the Verlet velocity algorithm [45] at 300 K (canonical ensemble). Temperature control was achieved using the Berendsen thermostat [46]. The potential was determined "on the fly" by means of the PM6 semiempirical Hamiltonian. The time step used for all simulations was 0.25 fs; total times of 0.5 and 4.0 ps were used in the equilibrium and production steps, respectively.

Results and discussion

Optimized structures and adsorption energies

We will start by discussing the interaction modes and stability of BPA on pristine graphene and graphene oxide (GO). As shown in Scheme 1, 10 BPA···adsorbent systems were analyzed: **1**, BPA adsorbed on pristine graphene; **2**–**7**, BPA adsorbed on the edges of GO models; **8**–**10**, adsorption of BPA on the basal plane (bulk) of oxidized graphene. Figures 1, 2, and 3 show the optimized geometries of **1**, **2**–**7**, and **8**–**9**, respectively. The optimized structures were related to the AE values to determine the most stable interaction modes and the roles of various functional groups in the physisorption strength. E_{vdW} corresponds to the contribution of dispersion forces to the AE. Table 1 shows values for the AE, E_{vdW}, and BSSE.

We first analyzed the physisorption of BPA on pristine graphene (Fig. 1). Three stable configurations were found. In **1a**, BPA interacts with the graphene bulk at a minimum distance of 2.36 Å, with phenol groups directed toward the surface to maximize π–π interactions while the methyl groups are directed away; the angle between the phenols is slightly increased by 0.85° compared to the angle of 108.67° seen in the isolated form of BPA. The AE is 13.66 kcal/mol. In **1b**, BPA is "seated" on the graphene surface at a distance of 2.76 Å; since one of the phenol rings is oriented perpendicular to the surface, vdW interactions are reduced, meaning that the AE is 1.45 kcal/mol lower than that for **1a**. Finally, in configuration **1c**, BPA is lying down on the graphene at a distance of 2.69 Å, with the angle between the phenols increased by 2.38° compared to that seen in the isolated form of BPA, allowing better contact between the π-clouds of the phenol rings and graphene. Physisorption is enhanced by 1.03 kcal/mol compared to that of **1a**.

Based on the results for the AE, the lying-down configuration (with an increase in the angle between the phenols) is the most stable for BPA on graphene because it maximizes the π–π stacking and dispersion forces between adsorbent and adsorbate. Zaib and co-workers have also reported that lying down is the lowest-energy configuration for the BPA–graphene system [26]; after performing calculations at the B3LYP5-D3/6-31++G(d,p)//B3LYP5-D3/6-31G level of theory, they reported an adsorption energy of 22.5 kcal/mol for BPA adsorbed on pristine graphene, although they did not use BSSE correction, and graphene was kept fixed during geometry optimization, so their value for the adsorption strength may have been slightly overestimated.

Figure 2 shows the interactions of BPA with various functional groups at the edges of GO models (**2**–**7**); in these cases, hydrogen-bond interactions between the hydroxyl groups of BPA and the functional groups at the edges of oxidized graphene predominate. In **2**, hydrogen bonds (1.76 and 1.69 Å) are established with carboxyl groups; the AE of 18.04 kcal/mol indicates that adsorption is enhanced by the functional groups with respect to **1**. Carbonyl or hydroxyl is combined with a carboxyl group in **3** and **4**, respectively, resulting in a decrease in the interaction strength of ~5 kcal/mol. In the next system, **5**, hydrogen bonds between BPA and the carbonyl groups (1.60 and 1.72 Å) suggest that the physisorption of BPA on these groups is stronger than it is on carboxyl groups; in fact, AE is 5.71 kcal/mol higher than it is for **2**. The combination of hydroxyl and epoxide groups in **6** leads to an AE of 17.18 kcal/mol, with hydrogen bond lengths of 1.61 and 1.97 Å; in this case, physisorption is mainly enhanced because BPA is slightly displaced

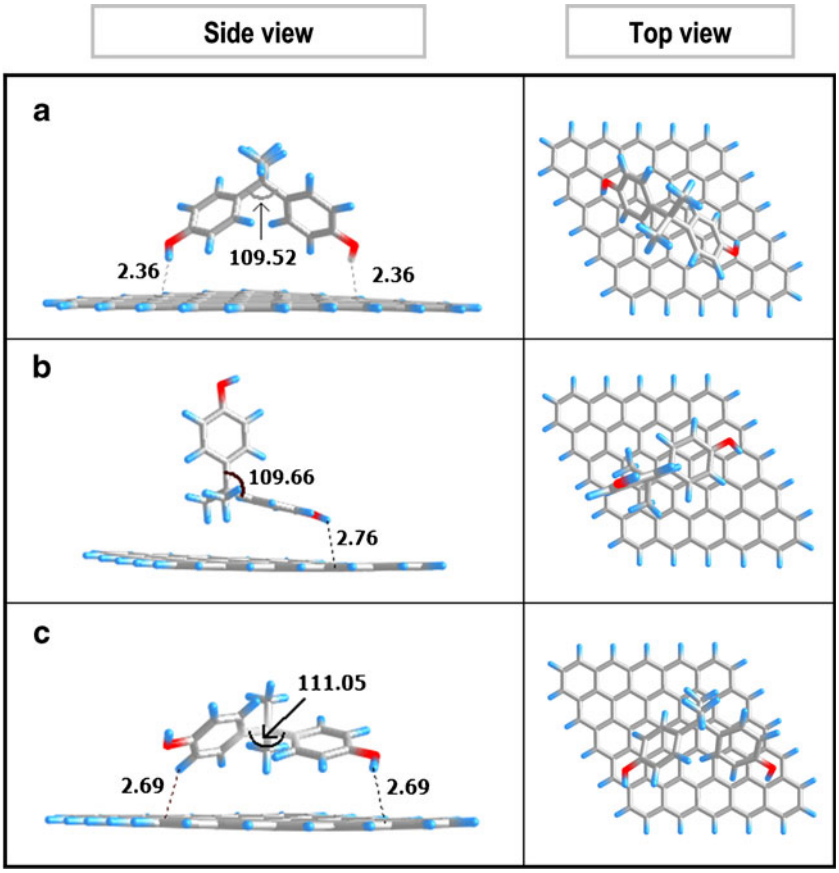

Fig. 1 Optimized molecular structures for BPA···graphene assemblies obtained at the PBE-D3/DZP level of theory; three interaction modes were obtained (**1a**, **1b**, **1c**). Angles are in degrees (°) and distances are in angstroms (Å). Color code by atom: *gray* carbon, *red* oxygen, *sky blue* hydrogen

toward the bulk of the adsorbent, allowing π–π or vdW interactions. On the other hand, the interaction mode proposed by Xu et. al. [25] is modeled in system **7**; in this case, the AE (11.87 kcal/mol) is less than those for **2** and **5** because OH functionalization is more stable on the basal plane of graphene, which is in accord with experimental evidence [27–31]. Slightly larger hydrogen bonds of 1.85 and 1.90 Å are found, in agreement with a decrease in AE. Results indicate that the physisorption of BPA at the edges of oxidized graphene (or on the remaining functional groups in reduced graphene oxide) is enhanced at sites containing two carbonyl or carboxyl groups; besides, the physisorption strength is even less on the hydroxyl groups (as proposed by Xu and co-workers) than on pristine graphene, indicating that this interaction mode is not the most stable configuration of BPA on graphene oxide.

We then analyzed the physisorption of BPA on the basal plane of graphene oxide (Fig. 3). In all cases (**8**–**10**), it was found that BPA is lying down on the adsorbents, as in **1c**. Physisorption is improved by hydrogen bonding, π–π stacking, and dispersion forces. In **8**, hydrogen bonds with lengths of 1.80 and 1.86 Å were established, with an AE of 21.50 kcal/mol (an increase of ~7 kcal/mol with respect to that of **3**). In **9**, physisorption is enhanced by ~2 kcal/mol by replacing epoxide with hydroxyl, indicating that hydroxyl groups in the GO basal plane are more suitable for BPA physisorption. Based on the previous result, an increase in AE was expected for **10**, which is in good agreement with the increase of ~3 kcal/mol over the interaction in **8**. In addition, the angle between the phenols increased by 4°, allowing improved vdW interactions and stacking between the phenol rings and the adsorbents. These results show that BPA physisorption is highly enhanced in the basal plane by the presence of hydroxyl and epoxide groups, indicating that oxidized graphene is a preferable adsorbent for BPA removal.

On the other hand, the vdW interaction energy is a good indicator of the importance of dispersion forces in the adsorbate–adsorbent system beyond chemical intuition. E_{vdW} values are listed in Table 1.

For systems **1a**–**c**, the stability of the adsorption is 100 % due to dispersion forces; vdW interactions increase in the order **1a**<**1b**<**1c**. As also deduced previously, the lying-down mode (**1c**) is the most stable because it leads to enhanced π–π interactions; in **1c**, E_{vdW} is increased by 5.51 (2.87) kcal/mol with respect to that of **1a** (**1b**). Note that differences between AE and E_{vdW} are due to antibonding contributions, which increase as nonbonding interactions increase.

Although the physisorption of BPA on the edges of oxidized graphene mainly occurs due to hydrogen-bond interactions, E_{vdW} indicates that vdW interactions contribute a little to the AE. For the most stable structures (**2** and **5**), the interaction is strengthened by ~28 % by dispersion forces. In

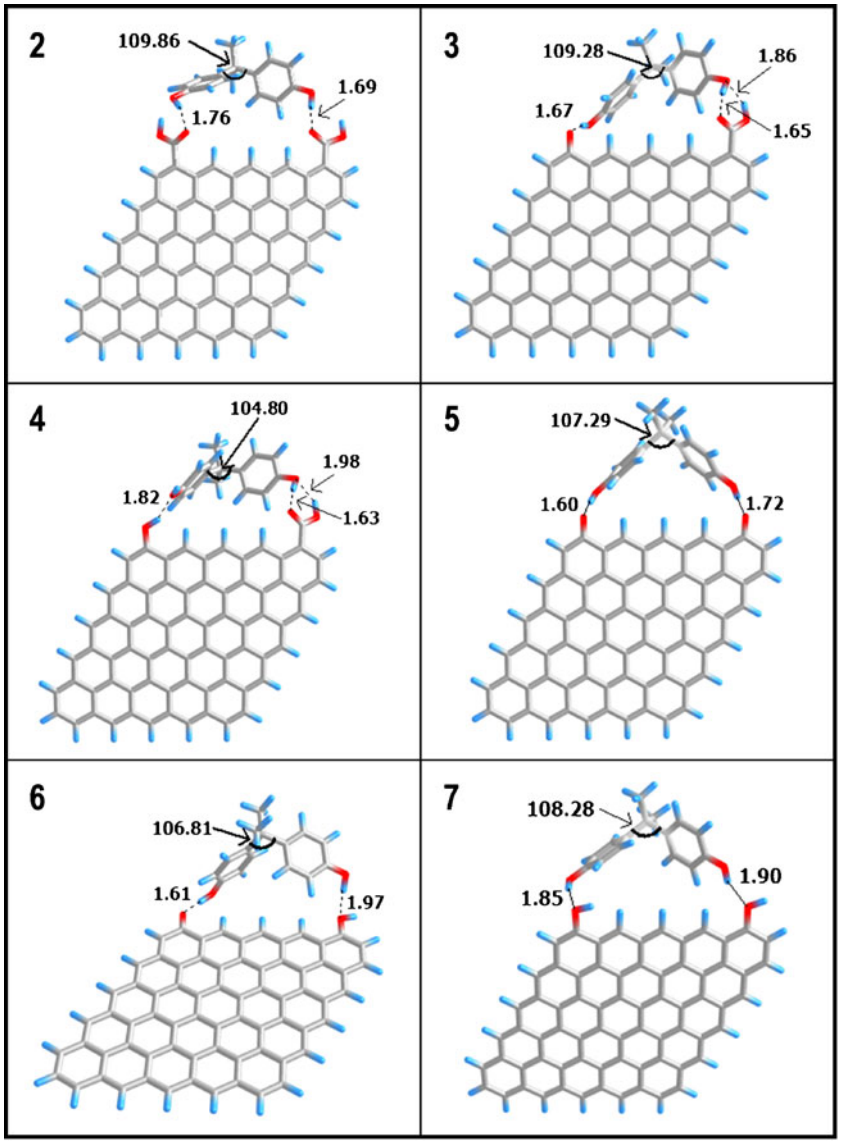

Fig. 2 Optimized molecular structures for BPA···oxidized (at the edges) graphene assemblies obtained at the PBE-D3/DZP level of theory. Angles are in degrees (°) and distances are in angstroms (Å). Color code by atom: *gray* carbon, *red* oxygen, *sky blue* hydrogen

structures **3**, **4**, **6**, and **7**, E_{vdW} values are similar to those found for **2** and **5**, so the hydrogen-bond interactions in these cases are less strong than those with two epoxide or two carboxyl groups, and dispersion forces improve the adsorption strength by 56 %. This reaffirms that physisorption at edges is enhanced by the presence of carboxyl or carbonyl groups, but interactions with other functional groups decrease the strength of the hydrogen bonds.

As mentioned before, BPA adsorption in the bulk of graphene oxide (**8**–**10**) is found to be highly enhanced by hydrogen bonds and π–π interactions. Moreover, E_{vdW} indicates that dispersion forces play the dominant role in the physisorption (contributing over 78 % of the interaction strength). In **8** (**9**), the vdW contribution is about 84 % (78 %). With respect to **10**, it was deduced previously that increasing the angle between the phenols by 4° improves the π–π coupling between the phenol rings and the graphene surface, which is in good agreement with the increase in E_{vdW}; in this case, vdW interactions contribute 94 % of the AE.

Finally, it is worth noting that BBSE values were generally larger when BPA was adsorbed on the edge and the basal plane of oxidized graphene, being on average ~9 kcal/mol (edge) and ~10 kcal/mol (basal plane). In pristine graphene, BSSE averages ~5 kcal/mol. This suggests that counterpoise correction must be adopted in related studies in order to ensure that the adsorption energies are not overestimated.

Physisorption stability

In order to check the stability of the BPA–graphene systems, we carried out molecular dynamics calculations on the most stable structures according to the AE: **1c**, **2**, **5**, **8**, **9** and **10**. We monitored the intermolecular distances during trajectories by means of the radial pair distribution function (g_{ab}), which allowed

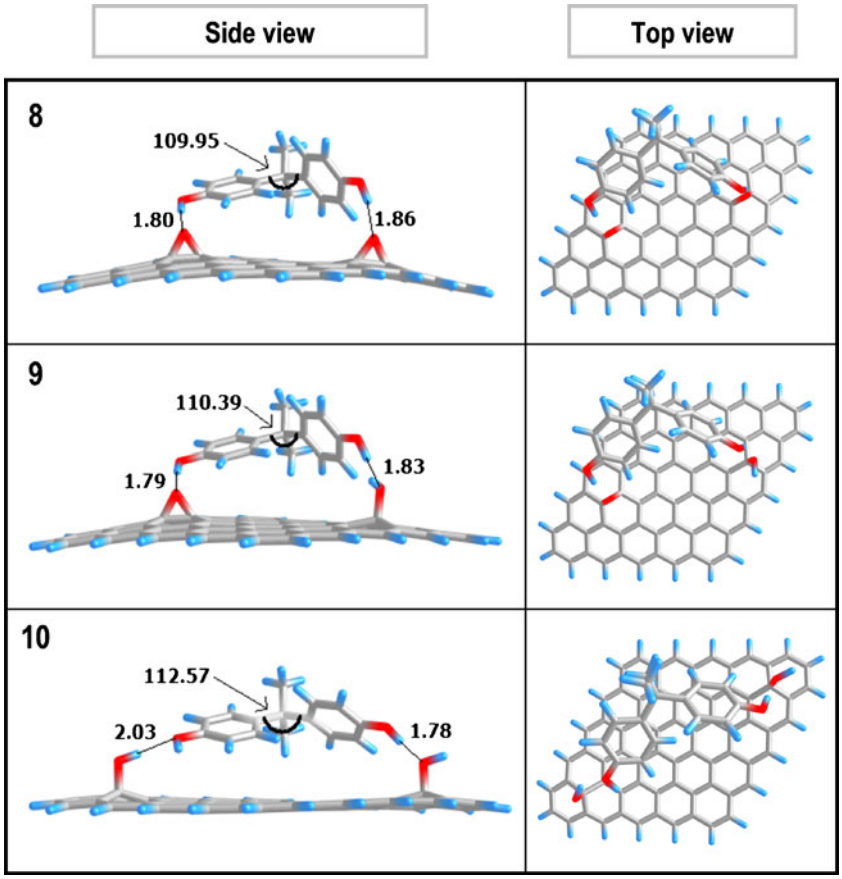

Fig. 3 Optimized molecular structures for BPA···oxidized (in the bulk) graphene assemblies obtained at the PBE-D3/DZP level of theory. Angles are in degrees (°) and distances are in angstroms (Å). Color code by atom: *gray* carbon, *red* oxygen, *sky blue* hydrogen

us to determine the distribution of the distances between two atoms within a given volume. The conservation of intermolecular distances is a good indication that physisorption is stable under dynamic conditions. Figure 4 shows the g_{ab} functions for the most stable complexes. Since there were a wide range of intermolecular distances, we considered the most representative ones, and obtained the distributions for over 40 conformations (on a total of 16,000) (Fig. S4 in the ESM shows the evolution of the geometry during the molecular dynamics calculations).

For **1c**, g_{ab} shows the intermolecular BPA···graphene distance. As observed in Fig. 1, the stationary distance for the optimized structure was 2.69 Å; during the production step, the

Table 1 Properties of adsorbent···BPA systems: adsorption energy (AE), contribution of van der Waals interactions to the AE (E_{vdW}), charge on BPA after physisorption (Q_{BPA}), and electrophilicity (ω). All properties were obtained at the PBE-D3/DZP level of theory

Adsorbent–asdorbate system	AE[a]	E_{vdW}[a]	BSSE[a]	Q_{BPA}	ω[c]
With pristine graphene					
1a: G···BPA_a	13.66	15.44 (100 %)[b]	5.16	0.03	27.61 (26.77)[c]
1b: G···BPA_b	12.21	18.08 (100 %)	4.30	0.04	26.89 (26.77)
1c: G···BPA_c	14.69	20.95 (100 %)	4.97	0.04	27.01 (26.77)
Wth functionalized graphene at the edges (L)					
2: $G^{L\text{-}COOH\text{-}COOH}$···BPA	18.04	5.03 (28 %)	9.23	−0.09	34.22 (31.43)
3: $G^{L\text{-}COOH\text{-}O}$···BPA	12.55	6.98 (56 %)	13.28	−0.08	35.77 (19.65)
4: $G^{L\text{-}COOH\text{-}OH}$···BPA	12.77	7.08 (55 %)	10.38	0.02	31.25 (30.76)
5: $G^{L\text{-}O\text{-}O}$···BPA	23.75	6.32 (27 %)	7.45	0.06	93.47 (56.25)
6: $G^{L\text{-}OH\text{-}O}$···BPA	17.18	7.70 (45 %)	7.74	−0.09	18.21 (14.06)
7: $G^{L\text{-}OH\text{-}OH}$···BPA	11.87	6.32 (53 %)	6.59	−0.09	28.10 (25.67)
With functionalized graphene in the bulk					
8: $G^{O\text{-}O}$···BPA	21.50	17.98 (84 %)	9.88	−0.08	26.04 (21.70)
9: $G^{OH\text{-}O}$···BPA	23.30	18.14 (78 %)	10.31	−0.08	16.19 (13.13)
10: $G^{OH\text{-}OH}$···BPA	24.28	22.92 (94 %)	11.18	−0.03	32.56 (31.23)
BPA					1.15

[a]Units of kcal/mol

[b]Contribution of vdW interactions to the AE as a percentage

[c]Corresponding ω value for the adsorbent in isolated form is shown in parentheses in eV

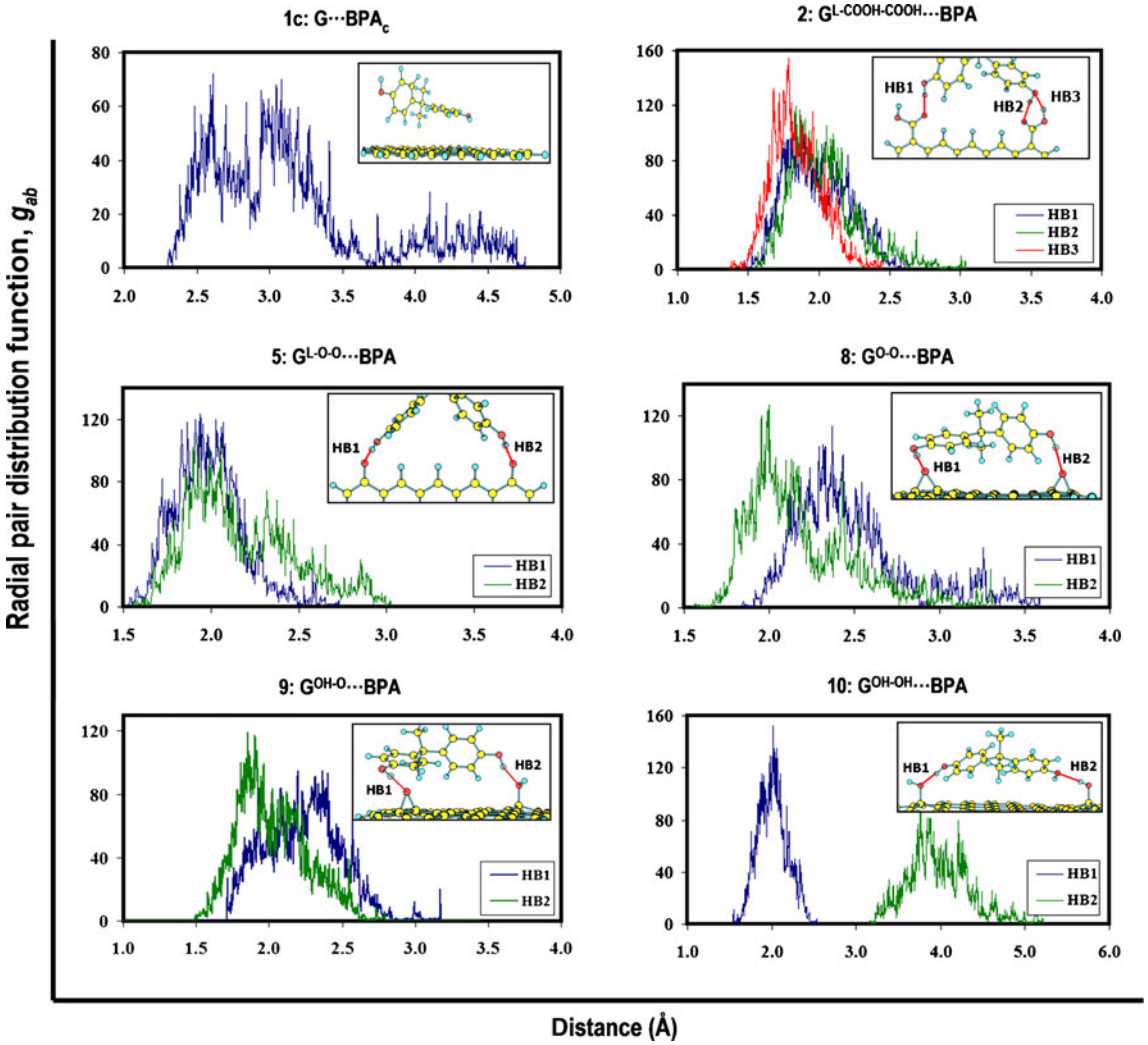

Fig. 4 Radial pair distribution function (g_{ab}) of intermolecular distances in systems **1c**, **2**, **5**, **8**, **9**, and **10**. *HB* hydrogen bond

intermolecular distance generally stayed within the range 2.5–3.5 Å, allowing interactions via dispersion forces and indicating that the physisorption is stable even under dynamic conditions. It is interesting to note that the lying-down mode of BPA on graphene was conserved during the production step.

For the edge-functionalized systems (**2** and **5**), the results again show that the physisorption of BPA on the adsorbent is stable. In **2**, three hydrogen bonds were analyzed, and it was found that these interactions between hydroxyl groups (of BPA) and carboxyl groups (of graphene) are well conserved, with peaks at 1.6–2.3 Å. Similar results were obtained for **5**, with intermolecular distances remaining within the range 1.7–2.3 Å; however, during trajectories, HB2 had peaks at 2.3–3.0 Å, suggesting that HB2 is a little weaker than HB1.

Regarding systems **8**–**9** (where BPA is adsorbed on the bulk of oxidized graphene), the lying-down disposition of BPA on oxidized graphene was retained during trajectories. In **8**, HB2 is stronger than HB1, with the main peaks occurring at 1.8–2.3 Å, while HB2 mainly varies within the range 2.1–2.7 Å. In **9**, hydrogen bonds are established with the respective epoxide and hydroxyl groups at the surface of graphene oxide, while g_{ab} shows that the hydrogen-bond distances are conserved during trajectories, in accord with the high stability indicated by the AE. Specifically, HB1 and HB2 stay mainly within the ranges 1.7–2.3 and 1.9–2.5 Å, respectively.

Finally, in **10**, HB1 was observed to remain between 1.9 and 2.1 Å, but HB2 was larger than HB1 (>3.15 Å); however, BPA adsorption would be even stable with a hydrogen bond due to the high contribution of vdW interactions (94 %), as noted previously.

Charge density distribution

The influence of BPA physisorption on the charge density distributions of graphene and graphene oxide was also studied. Focusing on the net charge on BPA (Q_{BPA}) (Table 1), a negative value indicates that BPA gains electrons, while a

positive value indicates that the graphene (or graphene oxide) surface gains electrons. In all cases, Q_{BPA} shows that changes in the charge density distribution due to BPA adsorption are on the order of 10^{-2} electrons, indicating that, in all of the models, the adsorption of BPA on graphene is not a charge-transfer interaction.

Molecular electrostatic potential (MEP) surfaces (Fig. 5) are useful for analyzing charge-controlled interactions (such as hydrogen bonds), as they reveal the charge density distributions in the isolated systems and allow us to elucidate the mechanism of physisorption [47]. As the MEP shows, the charge is localized in BPA, with negative charge on the oxygen atoms (−0.22) and the second carbon of the propane section (–0.39), while positive charge is localized on the methyl groups (0.15) and hydrogens of the hydroxyl groups (0.16) (values in parentheses show the Mulliken charge on each fragment). As noted before, in systems **1a**–**1c**, the disposition of BPA on graphene determines the increase in AE; graphene is a strong electron acceptor due to its large π-system, so it would favor configurations that allow it to interact with the negatively charged sites of BPA. This assumption is in good agreement with the results: in **1a**, the interaction occurs with the negatively charged hydroxyl groups of BPA; in **1b**, the seated mode of BPA allows graphene to interact with the negatively charged site of the propane section (which is more negative than the hydrogens of the hydroxyl groups), improving the AE; and in **1c**, adsorption is enhanced because the lying-down configuration of BPA allows the surface of graphene to interact with the most negatively charged sites of BPA, enhancing the AE. Thus, in addition to vdW/π–π interactions, charge-controlled interactions are important in the physisorption of BPA on the basal plane of graphene, albeit to a lesser degree than other interactions.

In the MEP surfaces of adsorbents based on graphene oxide, the functional groups are negatively charged because they accept electrons and due to the high electronegativity of oxygen with respect to carbon [3.44 vs 2.55, respectively, according to the Pauling scale]. In systems functionalized at the edges (**2**–**7**), charge-controlled interactions dominate, allowing hydrogen bonding between the hydroxyl groups of BPA (positively charged hydrogens) and the functional groups of graphene oxide (negatively charged oxygens). It is important to note that the hydroxyl groups of graphene oxide are less negative than the other functional groups, which explains the low AE values of and relatively long hydrogen bonds in **4**, **6**, and **7**.

Regarding BPA physisorption on the bulk of graphene oxide (**8**–**10**), the negatively charged oxygen atoms of oxidized graphene allow interaction with BPA via hydrogen bonds. In addition, as in **1c**, the lying-down disposition enhances charge-controlled interactions between the surface of graphene oxide (which accepts electrons) and the negatively charged sites of BPA.

Reactivity

The electrophilicity index (ω) for each system is shown in Table 1. It is apparent that all of the systems become more electrophilic after BPA adsorption (with respect to graphene

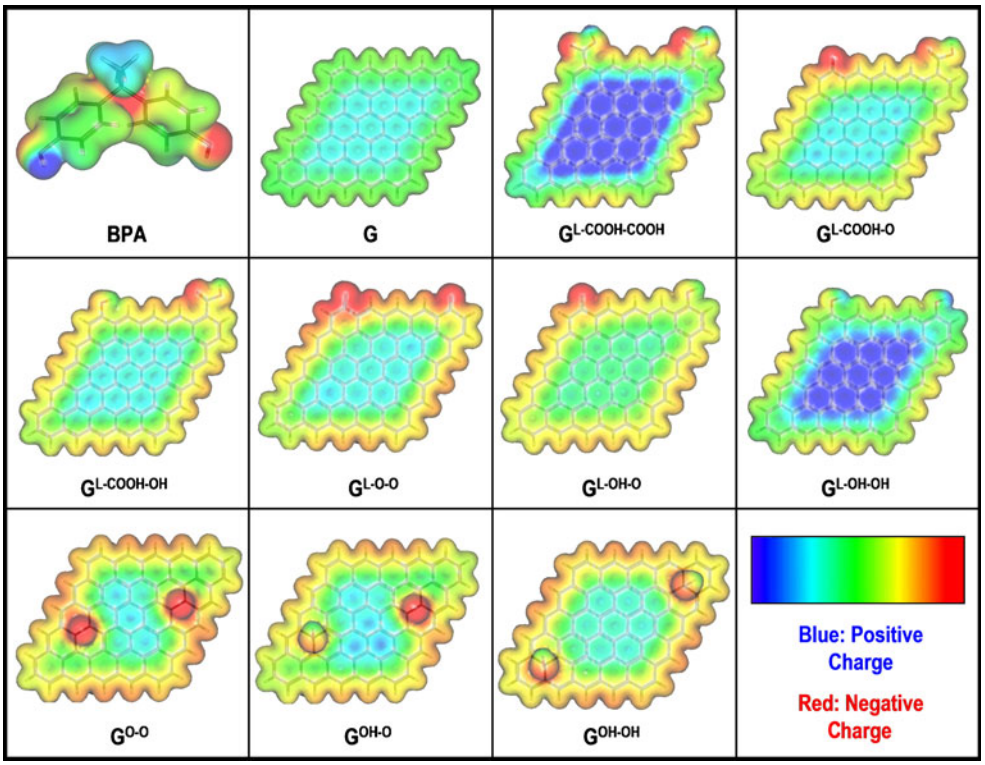

Fig. 5 Molecular electrostatic potential (MEP) surfaces for the BPA, pristine graphene, and graphene oxide models

and/or BPA in their isolated forms). The high electrophilicity of **5** (93.47 eV) may be due to its open-shell structure (with the unpaired electron localized on BPA, in accordance with its SOMO surface, Fig. 6). In addition, in all of the systems, the LUMO is mainly located on pristine graphene or graphene oxide, so the adsorbent is the electron acceptor, in agreement with the electron-accepting character of graphene. This means that increasing the electrophilic character of the adsorbent enhances its activity as an oxidant of BPA, implying that these are useful materials for the electrochemical degradation and detection of BPA.

Note that this donor–acceptor reactivity is related to frontier-controlled interactions (such as redox reactions, where experimental conditions are important), so this remark does not necessarily apply to Q_{BPA}. Nevertheless, experimental and/or electron transport calculations (such as those based on Green's function formalism) must be carried out to study the performance of graphene and graphene oxide in the detection of BPA and ECDs.

Conclusions

In summary, we carried out a computational study to investigate the physisorption of BPA on pristine graphene and graphene oxide. This study furthers understanding of the interaction modes of BPA on graphene adsorbents, and the roles of various functional groups in the adsorption strength.

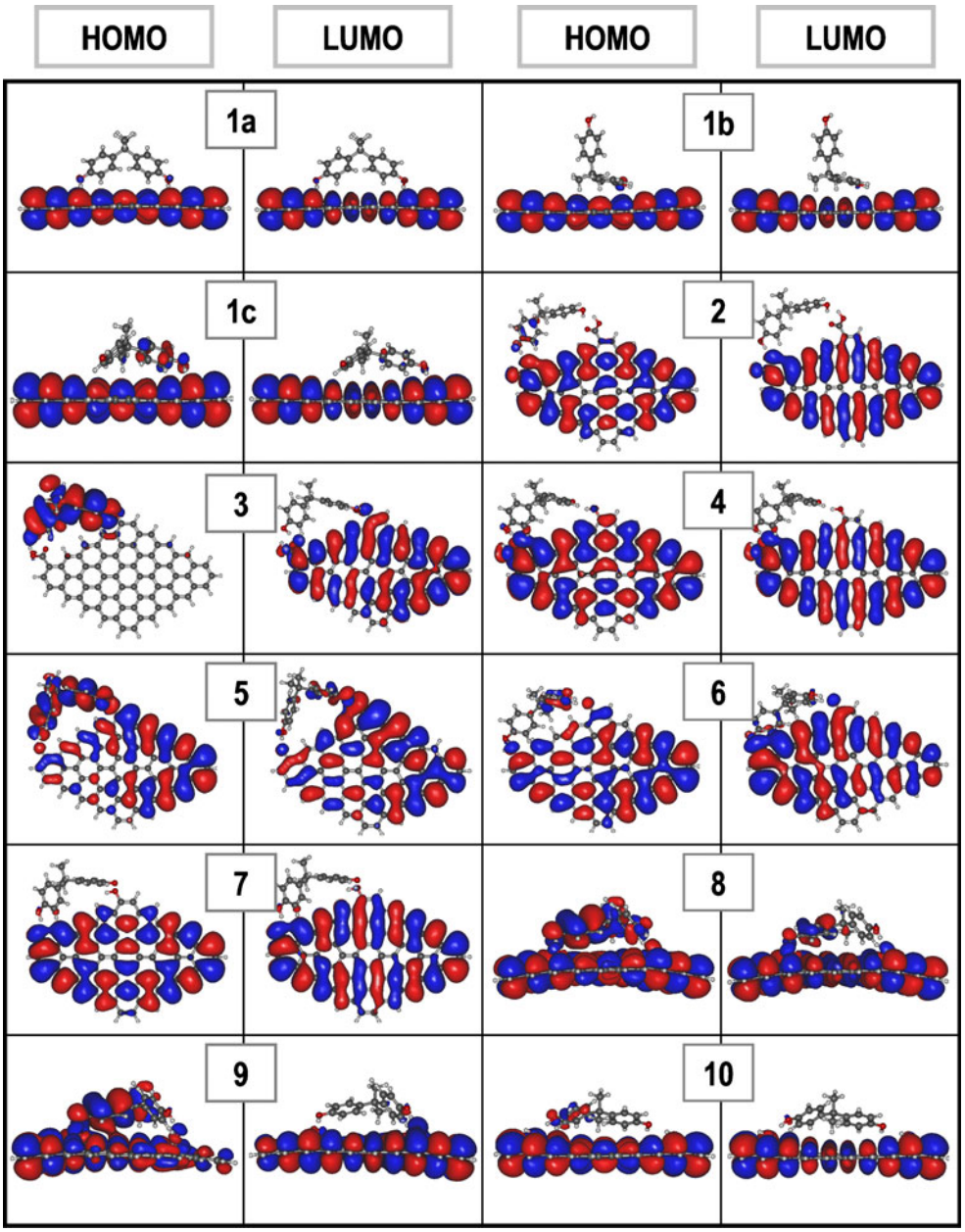

Fig. 6 HOMO and LUMO surfaces for systems **1**–**10**. HOMO is singly occupied in **3**, **6**, and **9**, meaning that it is the SOMO

Density-functional results were obtained at the PBE-D3 level (including dispersion force corrections). Three interaction modes for the BPA···graphene interaction were found, among which a lying-down disposition of BPA on graphene is the most stable since it maximizes the dispersion forces and π–π stacking. In addition, the adsorption of BPA at the edges of oxidized graphene is enhanced when carboxyl or carbonyl groups are present, but interactions with hydroxyls (or combinations of functional groups) decrease the strength of the hydrogen bonds. The strongest adsorption occurred at the basal plane of graphene oxide due to the presence of dispersion forces and π–π coupling (which provide the main contribution to the adsorption strength) as well as hydrogen bonds (which provide a smaller contribution), indicating that oxidized graphene is a better candidate than pristine graphene for a BPA removal agent. Additionally, the lying-down configuration enhances charge-controlled interactions because the basal plane of graphene (the electron acceptor) is near to the negatively charged sites of BPA. The charge-transfer mechanism for the BPA···graphene interaction was analyzed, but it was found to be insignificant because changes in the electronic population were on the order of 10^{-2} electrons after physisorption for all of the adsorbent–adsorbate systems. On the other hand, an increase in the electrophilicity of each system after the physisorption of BPA was observed (with respect to graphene and BPA in their isolated forms), with the adsorbent acting as the electron acceptor.

Finally, the stability of the adsorption of BPA on graphene and graphene oxide was demonstrated to be high by performing molecular dynamics calculations using the PM6 potential.

Acknowledgments The authors thank Juan M. Perez for the help provided in the last part of the article.

References

1. Staples CA, Dorn PB, Klecka GM, O'Block ST, Branson DR, Harris LR (2000) Bisphenol A concentrations in receiving waters near US manufacturing and processing facilities. Chemosphere 40(5):521–525. doi:10.1016/s0045-6535(99)00288-x
2. Belfroid A, van Velzen M, van der Horst B, Vethaak D (2002) Occurrence of bisphenol A in surface water and uptake in fish: evaluation of field measurements. Chemosphere 49(1):97–103. doi:10.1016/s0045-6535(02)00157-1
3. Santhi VA, Sakai N, Ahmad ED, Mustafa AM (2012) Occurrence of bisphenol A in surface water, drinking water and plasma from Malaysia with exposure assessment from consumption of drinking water. Sci Total Environ 427–428:332–338. doi:10.1016/j.scitotenv.2012.04.041
4. Varayoud J, Ramos JG, Bosquiazzo VL, Muñoz-de-Toro M, Luque EH (2008) Developmental exposure to bisphenol A impairs the uterine response to ovarian steroids in the adult. Endocrinology 149(11):5848–5860. doi:10.1210/en.2008-0651
5. Vandenberg LN, Hauser R, Marcus M, Olea N, Welshons WV (2007) Human exposure to bisphenol A (BPA). Reprod Toxicol 24(2):139–177. doi:10.1016/j.reprotox.2007.07.010
6. Mielke H, Gundert-Remy U (2009) Bisphenol A levels in blood depend on age and exposure. Toxicol Lett 190(1):32–40. doi:10.1016/j.toxlet.2009.06.861
7. Muñoz-de-Toro M, Markey CM, Wadia PR, Luque EH, Rubin BS, Sonnenschein C, Soto AM (2005) Perinatal exposure to bisphenol A alters peripubertal mammary gland development in mice. Endocrinology 146(9):4138–4147. doi:10.1210/en.2005-0340
8. Sugiura-Ogasawara M, Ozaki Y, S-i S, Makino T, Suzumori K (2005) Exposure to bisphenol A is associated with recurrent miscarriage. Hum Reprod 20(8):2325–2329. doi:10.1093/humrep/deh888
9. Kandaraki E, Chatzigeorgiou A, Livadas S, Palioura E, Economou F, Koutsilieris M, Palimeri S, Panidis D, Diamanti-Kandarakis E (2011) Endocrine disruptors and polycystic ovary syndrome (PCOS): elevated serum levels of bisphenol A in women with PCOS. J Clin Endocrinol Metab 96(3):E480–E484. doi:10.1210/jc.2010-1658
10. Bae S, Kim JH, Lim Y-H, Park HY, Hong Y-C (2012) Associations of bisphenol A exposure with heart rate variability and blood pressure. Hypertension 60(3):786–793. doi:10.1161/hypertensionaha.112.197715
11. EU (2011) Commission Directive 2011/8/EU of 28 January 2011 amending Directive 2002/72/EC as regards the restriction of use of bisphenol A in plastic infant feeding bottles. OJEU 26:11–14
12. Bizkarguenaga E, Ros O, Iparraguirre A, Navarro P, Vallejo A, Usobiaga A, Zuloaga O (2012) Solid-phase extraction combined with large volume injection-programmable temperature vaporization–gas chromatography–mass spectrometry for the multiresidue determination of priority and emerging organic pollutants in wastewater. J Chromatogr A 1247:104–117. doi:10.1016/j.chroma.2012.05.022
13. Han W, Luo L, Zhang S (2012) Adsorption of bisphenol A on lignin: effects of solution chemistry. Int J Environ Sci Technol 9(3):543–548. doi:10.1007/s13762-012-0067-1
14. Sun Q, Li Y, Chou PH, Peng PY, Yu CP (2012) Transformation of bisphenol A and alkylphenols by ammonia-oxidizing bacteria through nitration. Environ Sci Technol 46(8):4442–4448. doi:10.1021/es204424t
15. Huang RX, Fang ZQ, Yan XM, Cheng W (2012) Heterogeneous sono-Fenton catalytic degradation of bisphenol A by Fe_3O_4 magnetic nanoparticles under neutral condition. Chem Eng J 197:242–249. doi:10.1016/j.cej.2012.05.035
16. Dimitroula H, Daskalaki VM, Frontistis Z, Kondarides DI, Panagiotopoulou P, Xekoukoulotakis NP, Mantzavinos D (2012) Solar photocatalysis for the abatement of emerging micro-contaminants in wastewater: synthesis, characterization and testing of various TiO_2 samples. Appl Catal B 117:283–291. doi:10.1016/j.apcatb.2012.01.024
17. Novoselov KS, Geim AK, Morozov SV, Jiang D, Zhang Y, Dubonos SV, Grigorieva IV, Firsov AA (2004) Electric field effect in atomically thin carbon films. Science 306(5696):666–669. doi:10.1126/science.1102896
18. Lee C, Wei X, Kysar JW, Hone J (2008) Measurement of the elastic properties and intrinsic strength of monolayer graphene. Science 321(5887):385–388. doi:10.1126/science.1157996
19. Chen S, Wu Q, Mishra C, Kang J, Zhang H, Cho K, Cai W, Balandin AA, Ruoff RS (2012) Thermal conductivity of isotopically modified graphene. Nat Mater 11(3):203–207. http://www.nature.com/nmat/journal/v11/n3/abs/nmat3207.html#supplementary-information
20. Bolotin KI, Sikes KJ, Jiang Z, Klima M, Fudenberg G, Hone J, Kim P, Stormer HL (2008) Ultrahigh electron mobility in suspended graphene. Solid State Commun 146(9–10):351–355. doi:10.1016/j.ssc.2008.02.024

21. Pumera M, Ambrosi A, Bonanni A, Chng ELK, Poh HL (2010) Graphene for electrochemical sensing and biosensing. TrAC Trends Anal Chem 29(9):954–965. doi:10.1016/j.trac.2010.05.011
22. Fan H, Li Y, Wu D, Ma H, Mao K, Fan D, Du B, Li H, Wei Q (2012) Electrochemical bisphenol A sensor based on N-doped graphene sheets. Anal Chim Acta 711:24–28. doi:10.1016/j.aca.2011.10.051
23. Ntsendwana B, Mamba BB, Sampath S, Arotiba OA (2012) Electrochemical detection of bisphenol a using graphene-modified glassy carbon electrode. Int J Electrochem Sci 7(4):3501–3512
24. Huang C, Wu Y, Chen J, Han Z, Wang J, Pan H, Du M (2012) Synthesis and electrocatalytic activity of 3Au–1Pd alloy nanoparticles/graphene composite for bisphenol A detection. Electroanalysis 24(6):1416–1423. doi:10.1002/elan.201100728
25. Xu J, Wang L, Zhu Y (2012) Decontamination of bisphenol A from aqueous solution by graphene adsorption. Langmuir 28(22):8418–8425. doi:10.1021/la301476p
26. Zaib Q, Khan I, Saleh N, Flora JV, Park Y-G, Yoon Y (2012) Removal of bisphenol A and 17β-estradiol by single-walled carbon nanotubes in aqueous solution: adsorption and molecular modeling. Water Air Soil Pollut 223(6):3281–3293. doi:10.1007/s11270-012-1109-5
27. Lerf A, He H, Forster M, Klinowski J (1998) Structure of graphite oxide revisited. J Phys Chem B 102(23):4477–4482. doi:10.1021/jp9731821
28. Cai W, Piner RD, Stadermann FJ, Park S, Shaibat MA, Ishii Y, Yang D, Velamakanni A, An SJ, Stoller M, An J, Chen D, Ruoff RS (2008) Synthesis and solid-state NMR structural characterization of ^{13}C-labeled graphite oxide. Science 321(5897):1815–1817. doi:10.1126/science.1162369
29. Schniepp HC, Li J-L, McAllister MJ, Sai H, Herrera-Alonso M, Adamson DH, Prud'homme RK, Car R, Saville DA, Aksay IA (2006) Functionalized single graphene sheets derived from splitting graphite oxide. J Phys Chem B 110(17):8535–8539. doi:10.1021/jp060936f
30. Cote LJ, Kim F, Huang J (2008) Langmuir−Blodgett assembly of graphite oxide single layers. J Am Chem Soc 131(3):1043–1049. doi:10.1021/ja806262m
31. Pandey D, Reifenberger R, Piner R (2008) Scanning probe microscopy study of exfoliated oxidized graphene sheets. Surf Sci 602(9):1607–1613. doi:10.1016/j.susc.2008.02.025
32. Stewart JJP (2012) MOPAC2012. Stewart Computational Chemistry, Colorado Springs. http://openmopac.net (2012).
33. Perdew JP, Burke K, Wang Y (1996) Generalized gradient approximation for the exchange-correlation hole of a many-electron system. Phys Rev B 54(23):16533–16539
34. Perdew JP, Burke K, Wang Y (1998) Erratum: Generalized gradient approximation for the exchange-correlation hole of a many-electron system [Phys. Rev. B 54, 16 533 (1996)]. Phys Rev B 57(23):14999–14999
35. Pramanik A, Kang HS (2011) Density functional theory study of O_2 and NO adsorption on heteroatom-doped graphenes including the van der Waals interaction. J Physl Chem C 115(22):10971–10978. doi:10.1021/jp200783b
36. Wuest JD, Rochefort A (2010) Strong adsorption of aminotriazines on graphene. Chem Commun 46(17):2923–2925
37. Tang S, Cao Z (2012) Adsorption and dissociation of ammonia on graphene oxides: a first-principles study. J Phys Chem C 116(15):8778–8791. doi:10.1021/jp212218w
38. Grimme S, Antony J, Ehrlich S, Krieg H (2010) A consistent and accurate ab initio parametrization of density functional dispersion correction (DFT-D) for the 94 elements H–Pu. J Chem Phys 132(15):154104
39. Neese F (2012) The ORCA program system. Wiley Interdiscipl Rev Comput Mol Sci 2(1):73–78. doi:10.1002/wcms.81
40. Allouche A-R (2011) Gabedit—a graphical user interface for computational chemistry softwares. J Comput Chem 32(1):174–182. doi:10.1002/jcc.21600
41. Cortes Arriagada D, Sanhueza L, Kerry W (2013) Removal of 4-chlorophenol using graphene, graphene oxide, and A-doped graphene (A = N, B): a computational study. Int J Quantum Chem (in press). doi:10:10.1002/qua.24416
42. Boys SF, Bernardi F (1970) The calculation of small molecular interactions by the differences of separate total energies. Some procedures with reduced errors. Mol Phys 19(4):553–566. doi:10.1080/00268977000101561
43. Parr RG, Lv S, Liu S (1999) Electrophilicity index. J Am Chem Soc 121(9):1922–1924. doi:10.1021/ja983494x
44. Chattaraj PK, Sarkar U, Roy DR (2006) Electrophilicity index. Chem Rev 106(6):2065–2091. doi:10.1021/cr040109f
45. Verlet L (1967) Computer "experiments" on classical fluids. I. Thermodynamical properties of Lennard–Jones molecules. Phys Rev 159(1):98–103
46. Berendsen HJC, Postma JPM, Gunsteren WF, DiNola A, Haak JR (1984) Molecular dynamics with coupling to an external bath. J Chem Phys 81(8):3684–3690
47. Cortés Arriagada D (2013) Global and local reactivity indexes applied to understand the chemistry of graphene oxide and doped graphene. J Mol Model 19:919–930. doi:10.1007/s00894-012-1642-6